Searching for ring-like structures in the Cosmic Microwave Background

Searching for ring-like structures in the Cosmic Microwave Background

M. López [1,2], P. Bonizzi[3], K. Driessens[3], G. Koekoek[4], J. de Vries[4], R. Westra[3]
[1] *Institute for Gravitational and Subatomic Physics (GRASP), Department of Physics, Utrecht University, Princetonplein 1, 3584 CC Utrecht, The Netherlands.*
[2] *Nikhef, Science Park 105, 1098 XG Amsterdam, The Netherlands.*
[3] *Department of Data Science and Knowledge Engineering, Maastricht University, Maastricht, the Netherlands.*
[4] *Department of gravitational waves and fundamental physics, Faculty of Science and Engineering, Maastricht University, Maastricht, the Netherlands.*

In this research we present a new methodology to search for ring-like structures in the CMB. The particular context of this work is to investigate the presence of possible observational effects associated with Conformal Cyclic Cosmology (CCC), known as Hawking points. Although our results are not conclusive due to the statistical disagreement between the CMB sky map and the simulated sky maps in accordance to ΛCDM, we are able to retrieve ring-like anomalies from an artificial data at 95% confidence level. Once this discrepancy has been assessed, our method may be able to provide evidence of the presence or absence of Hawking points in the CMB. Hence, we stress the need to continue the theoretical and experimental research in this direction.

PACS numbers:

I. INTRODUCTION

Throughout the years, numerous theories and several experiments have been performed in order to answer one of the most fundamental questions of humanity: *what are the dynamics of the very early and very late Universe?* The resulting answer involves the Standard Cosmological model, ΛCDM, although there are some inconsistencies with other areas of physics that some speculative theories try to solve (see discussion in [18]). In this research we explore the observational implications in the Cosmic Microwave Background (CMB) of a theory of Sir Roger Penrose named Conformal Cyclic Cosmology (CCC) [19], whose latest statistical analyses have been under discussion [7, 15]. Moreover, we develop a method to assess its presence and potential location in the CMB. Even if the methodology developed in the present work is employed to search for anomalies in the CMB related to CCC, it can certainly be extended to other theories and different data sets.

The main premise of CCC is that the Universe is in a state of eternal inflation and its full evolution is divided in *aeons* that are separated from each other by conformal transformations at the *cross-over* [18, 19]. In a remote future all matter will either be captured in supermassive blackholes, that subsequently radiate into massless particles by *Hawking evaporation*, or, as it is postulated by CCC, will experience a mass fade out to become massless with time (see [7] for details). Eventually this remote and massless universe will be conformally indistinguishable from the start of a new universe. Penrose argues that this resemblance is not coincidental and as such, the end of a universe can be mapped to the beginning of a new universe, making the history of the Universe a (possibly endless) cycle of *aeons*.

Similarly to ΛCDM, every *aeon* described by CCC starts with a Big Bang and, due to the cosmological constant $\Lambda > 0$, ends with an exponential expansion in a remote future around $\sim 10^{100}$ years. The main differences between ΛCDM and CCC are that Penrose does not consider a model with early Universe *inflation*, and that the entire history of the Universe is taken to be a succession of *aeons*. In CCC, an *aeon* is defined as the start of the Universe and the end of it.

According to CCC there are two types of events from the previous *aeon* that could be observed today. One of these would be the effects of gravitational waves coming from inspiralling pairs of supermassive black holes and the other the effects of the evaporation of supermassive black holes, known as *Hawking points* (hereafter *"HPs"*). In this research we will focus our attention on the second type of events.

At the end of an *aeon*, mass-less particles are *squashed conformally* at the cross-over. Hence, all radiation from the evaporation of a black hole is concentrated into a HP, and it will travel into the subsequent *aeon* "heating" the matter of the early Universe, leaving imprints in the Cosmic Microwave Background (CMB). Due to relativistic constraints and given the known expansion of the universe, the imprints are expected in the form of a Gaussian-like distribution, which should be projected in the CMB as circular annuli that do not exceed an outer diameter of $\sim 4°$, corresponding to a maximum outer radius of ~ 0.035 radians [7].

To accept or reject CCC it is crucial to perform robust and strong analyses and statistical tests on the data from the CMB to verify the existence of HPs and their locations in the sky. The aim of this research is to search for anomalous annuli in the CMB temperature field data by comparing two different distributions: one population where HPs could potentially exist and another population where HPs are not present. The first population comes from the CMB sky map measured by *Planck* (hereafter *real CMB sky map*), while the second population is

obtained via simulations according to the Standard Cosmological theory ΛCDM (hereafter *simulated CMB sky map*).

This paper is organised as follows. A brief overview of related works is given in Section II. In Section III we describe the real data and the simulations of the CMB temperature field. Subsequently, we give a definition of our measurements (Section IV A), we provide a pseudocode of the algorithm to scan the CMB sky maps (Section IV B) and we describe the methodology employed to measure the quality of the simulations, the existence of HPs and their locations (Sections IV C, IV D and IV E). In Section V we report the results, showing the performance of our procedure. Finally, in Section VI we discuss the improvements of this work with respect to the current state-of-the-art and we conclude.

II. RELATED WORK: IMPRINTS OF THE PREVIOUS AEON

Several studies that test CCC have been conducted since Penrose presented his theory. Most of the studies aimed to indirectly detect gravitational waves produced by the collision of supermassive black holes in the previous aeon. It is theorized that collisions and formations of supermassive black holes would happen in the same galaxies due to the abundance of matter. As a consequence of several mergers in the same region, those remnants from the previous *aeon* should be projected in the CMB as concentric rings with an angular diameter $\leq 40°$. This type of events will not be discussed in this research but we can extrapolate some search methodologies to our research, so we briefly describe them in the following.

In [13], the authors explore Wilkinson Microwave Anisotropy Probe (WMAP) data to search for rings with low temperature variance according to a certain threshold and high population of annuli was encountered in some regions. The points selected in the CMB were centers of concentric rings and deviated 6σ along the annuli from the Gaussian expectation of ΛCDM. In [14], it is proposed the *sky-twist* methodology to test whether the numerous centres of multiple low-variance rings depended upon their being circular rather that some other shape, as the existence of elliptical shapes in WMAP sky map would contradict CCC. However, it was observed that low-variance ellipses where nonexistent in the data.

In [16] three different frequency bands with artificial Gaussian maps with the same harmonic spectrum are scanned and their results are compared, while in [6] it is presented the same study but with Planck data. The comparison was performed not with traditional statistical methods, but rather a new methodology proposed in [17], known as *A-functions* that are defined in Section IV C. Due to a high computational cost only 100 statistical artificial maps were scanned and the authors found ring-like structures with 99.7% confidence level.

In [3], the analysis of [13] with WMAP and Planck data is repeated. The authors performed the same procedure not only on real maps, but also in sky maps sampled from Gaussian distributions containing the usual CMB anisotropy power spectrum, which is consistent with the predictions of ΛCDM, and it was obtained the same results in both types of maps. Moreover, it is argued that the threshold chosen to select the low-variance rings in [13] was a particular search criterion and had no statistical significance.

In [21] it was implemented the same analysis as [16], but instead of employing the A-functions to compare the real distribution against an artificial distribution, the authors develop their own methodology based on matched filters and χ^2 statistics to compare both distributions. Due to their results the authors conclude that no imprints are present in the data.

Now, we describe the outcomes of studies that aimed to detect HPs. In [7], after scanning a real CMB sky map and 10.000 simulated maps, the authors claimed to have found HPs in the real sky map at 99.98% confidence level according to their metrics of [17], in favour of CCC. In [15], the authors report to have found HPs at 87% confidence level with the same metrics, concluding that this result is not significant enough. It is important to note that both studies employed large sky maps of $N_{\text{side}} = 1024$, where this parameter represents the resolution of the grid used according to Healpy [12]. Because this resolution translates into ≈ 12 million pixels it is crucial to understand the time complexity of their algorithms, which are not discussed in these works. Furthermore, the authors also do not discuss the reliability of their simulations with the real CMB sky map or the robustness of the A-functions from [17]. In this work we aim to address this question as well.

III. THE COSMIC MICROWAVE BACKGROUND TEMPERATURE FIELD

The CMB offers us a look at the universe when it was about 1/36.000 of its present age. At that time, the Universe became transparent, emitting photons that have traveled freely ever since. However, not all photons that arrive to our antennas belong to the CMB. The main astrophysical sources of noise come from our own Galaxy through different mechanisms: syncrotron radiation, free-free emission and spinning dust radiation that dominate at low frequencies, and thermal dust. It is true that the best frequencies to observe the CMB are around 70 GHz [7], but even if at this range of frequencies the contamination of the CMB signal is minimized, there are still systematic errors in the CMB temperature determination that are not taken into account. For these reasons, many cleaning techniques had been developed to remove the foregrounds from the sky maps obtained by telescopes such as Spectral Estimation Via Expectation Maximization (SEVEM), Needlet Internal Linear Combination (NILC), Spectral Matching Independent Compo-

nent Analysis (SMICA) and Commander - Ruler. In the present work we employ the full missions maps cleaned from *Planck* 2nd release[1], and we refer to them as the *real CMB sky maps*.

As we mentioned before, we want to compare a population were HPs are potentially present, namely the real CMB sky maps, with a population were HPs are guaranteed to not exist, i.e. simulated CMB sky maps in accordance with ΛCDM, to later compute their similarities or dissimilarities. Simulating the CMB temperature field is non-trivial, as this radiation encloses a large amount of information about the primordial Universe, which is strongly dependent on its shape and early composition. Fortunately, we can artificially obtain CMB sky maps with the Code for Anisotropies in the Microwave Background (CAMB) [4, 5]. With CAMB we are able to compute the angular power spectrum of the simulation $C_{\ell_{\rm sim}}$ according to the cosmological parameters obtained from *Planck 2018* [11], and with *Healpy* a temperature field is generated. From the possible values that multi-pole ℓ could acquire, we exclude ℓ_0 and ℓ_1 and we only expand the CMB until $\ell = 1500$, which it is expected to have a negligible effect on the temperature, as proposed in [7], from this point on-wards the scales represent noise. Due to the resolution of our maps being $N_{\rm side} = 1024$, to simulate Planck's camera resolution we smooth $C_{\ell_{\rm sim}}$ with a Gaussian beam at $fwhm = 10'$ according to [10] with *Healpy* package [8, 9].

Because we want to test the existence and the location of HPs in many simulated maps, we compute several artificial maps that come from the same angular power spectrum with *Healpy*. The code that generates the simulated maps needs to distribute the temperature field in accordance to ΛCDM, with the assumption that the CMB sky map is almost a Gaussian distribution. As the distribution occurs with a random seed, no two maps are alike and we can simulate the artificial maps recursively.

IV. THE METHODOLOGY

We propose a methodology to find ring-like anisotropies in the CMB. For this aim we compare two distributions of measurements: one where HPs could potentially exist (real CMB sky maps) and another one where they are not present (simulated CMB sky maps in accordance to ΛCDM). To construct both distributions we need to scan all the different sky maps from Section III and calculate a certain measurement m at each pre-defined sky location for annuli of different inner and outer radius $\{r_{\rm in}, r_{\rm out}\}$.

Once we have computed all the measurements m we need to perform statistical tests to understand if temperature fluctuations are expected by ΛCDM or are anomalies in accordance to CCC. For this second aim we measure the similarity or dissimilarity of both distributions of measurements m, in the region where HPs are expected according to CCC, ($r_{\rm out} \leq 0.035$ rad). Another crucial point is to assess the reliability of the simulations, i.e. we need to compare both distributions in the region where HPs are not expected under the assumption that they are similar ($r_{\rm out} \geq 0.035$ rad). Furthermore, if HPs were to be present in the real CMB sky maps, we would locate them to compare them against the ones found in [7].

This section is structured as follows: we provide a clear definition of the measurements m employed in IV A and we present a pseudo-code of the scanning algorithm in IV B. In IV C we give an overview of different statistical tests and its hypotheses. Moreover, we assess the performance of the algorithm with an artificial data set as we explain in Section IV D. In Section IV E we present a methodology to compute the locations of HPs in the real CMB sky map, if we were to find a positive proof of their existence.

A. Measuring the slope

According to CCC, HPs present a Gaussian-like distribution, but in the real CMB sky map they would be reflected as 2-dimensional annuli, whose temperature gradient monotonically decreases as we move away from the center. Due to the fact that temperature variations are very small, the gradient should diminish slowly and we can approximate it to a linear relationship between the temperature T and the angular distance d from the center. With this idea in mind, several authors search for negative slopes of the temperature around given sky directions (see [7] and [15] for details). HPs should have the most negative normalized slopes of the population, but it is not known *how negative*.

To find such slopes we can employ common least squares, where we define a as the slope of this linear relationship and b as the intercept of the line $T = ad + b$. Because we intend to scan the CMB sky maps to search for annuli of different sizes $\{r_{\rm in}, r_{\rm out}\}$, one needs to appreciate the change in size implies a change in the number of pixels and hence different variances for the slope. To take this into account, in [7] the authors define the measurement needed to search for HPs as the normalized slope, i.e. $\hat{a} = a/\sigma_a$, where σ_a is the standard deviation of the distribution of annuli with given $r_{\rm in}$ and $r_{\rm out}$. In this research we also use the Pearson correlation coefficient r as a measurement to search for HPs, because the whole measurement of a HP depends on the assumption that the angular distance d and T are linearly correlated.

In short, the measurements employed in this research are normalized slopes $\hat{a}$ and Pearson coefficients r.

[1] They can be downloaded from Infrared Science Archive on Planck Public Data Release 2 [2]

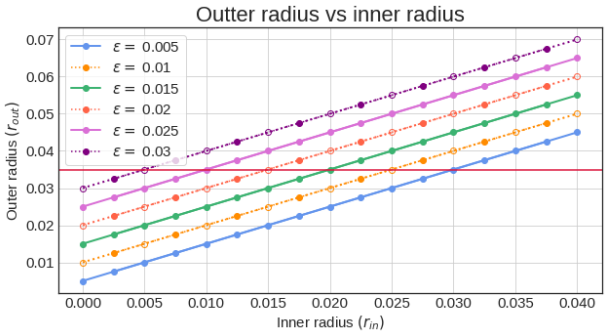

FIG. 1: Range of annuli explored in this research. Here, we define the width as $\epsilon = r_{\rm in} - r_{\rm out}$. The red horizontal line corresponds to the theoretical upper bound for the $r_{\rm out}$ of HPs. Empty bullets in dashed lines correspond to sizes explored in [7]. In our search we additionally include the sizes shown as filled bullets.

B. Scanning the CMB

Due to the large amount of pixels that each map has ($\approx$ 12.5 million), and the amount of maps and annuli that we need to explore (1004 sky maps and different sizes of annuli), it is essential to optimize the performance of our algorithm. To this end, we employ *Healpy* and *Numba* packages [8, 9, 20]. To illustrate our search we plot in Fig. 1 the sizes of the annuli in consideration. Below, we provide a pseudo-code of the algorithm.

Algorithm 1 Computation of measurement m

Require: Temperature T, c centers, annulus size $\{r_{\rm in}, r_{\rm out}\}$.
Initialise $M = \emptyset$
for all c **do**
  for all $\{r_{\rm in}, r_{\rm out}\}$ **do**
    if $\mathcal{A}(c, r_{\rm in}, r_{\rm out}) \cap$ *galactic center* $= \emptyset$ **then**
      Get pixels:
        $\mathcal{P}(c, r_{\rm in}, r_{\rm out}) =$ sky map $\cap\, \mathcal{A}(c, r_{\rm in}, r_{\rm out})$
      Get temperatures $T(\mathcal{P}(c, r_{\rm in}, r_{\rm out}))$
      Calculate angular distances $d(\mathcal{P}(c, r_{\rm in}, r_{\rm out}))$
      Calculate the measurement $m(c, r_{\rm in}, r_{\rm out})$
      $M = M \cup \{m(c, r_{\rm in}, r_{\rm out}\}$
    end if
  end for
end for
return M

The task of Algorithm 1 is to scan a sky map, calculating the measurement m for each pre-defined annulus, defined as

$$\mathcal{A}(c, r_{\rm in}, r_{\rm out}) \equiv \{x \in \mathcal{X} \mid r_{\rm in} < |x - c| < r_{\rm out}\}, \qquad (1)$$

for a given center $c = \{l,\ b\}$ and a certain inner and outer radius $\{r_{\rm in}, r_{\rm out}\}$. Because the sky maps are in galactic coordinates, l represents the galactic longitude and b the galactic latitude. Thus, $\mathcal{X} = \{0 < l < 2\pi, -\frac{\pi}{4} < b < \frac{\pi}{4}\}$. In this search we scan around 12800 pre-defined centers c that lay outside the *galactic center*[2], $l = [-\frac{\pi}{9}, \frac{\pi}{9}]$, to avoid undesired contributions from the Milky Way galaxy. Furthermore, annuli that happen to intersect this region get discarded. At each location we obtain the pixels of annuli with different sizes $\{r_{\rm in}, r_{\rm out}\}$,

$$\mathcal{P}(c, r_{\rm in}, r_{\rm out}) = \textit{sky map} \cap \mathcal{A}(c, r_{\rm in}, r_{\rm out}). \qquad (2)$$

Computationally this operation is performed by obtaining the pixels of the inner circle,

$$\mathcal{P}_{in}(c, r_{\rm in}) = \textit{sky map} \cap \{x \in \mathcal{X} \mid r_{\rm in} < |x - c|\}, \qquad (3)$$

and similarly, the pixels from outer circle $\mathcal{P}_{out}$ to get the intersection $\mathcal{P}(c, r_{\rm in}, r_{\rm out}) = (\mathcal{P}_{in}(c, r_{\rm in}) \cap \mathcal{P}_{out}(c, r_{\rm out}))'$. We obtain the temperature of the pixels $T(\mathcal{P}(c, r_{\rm in}, r_{\rm out}))$ and the angular distance $d(\mathcal{P}(c, r_{\rm in}, r_{\rm out}))$ from pixel to the center c.[3]

We normalize the slope as $\hat{a} = a/\sigma_a$, where σ_a refers to the standard deviation of the slopes of all the annuli that belong to the same family (see Section IV A for details). We define a family of annuli $\mathscr{A}(r_{\rm in}, r_{\rm out})$ to be the set of all annuli with the same size but different centers c,

$$\mathscr{A}(r_{\rm in}, r_{\rm out}) \equiv \{\mathcal{A}(c, r_{\rm in}, r_{\rm out}) \ \mid \forall\ c\}, \qquad (4)$$

and $\sigma_a = \sigma(\mathscr{A}(r_{\rm in}, r_{\rm out}))$. Finally, we calculate our measurement $m(c, r_{\rm in}, r_{\rm out})$. Because we have two types of measurements, namely the slope a and the Pearson coefficient r, we calculate $\hat{a} = m_1(c, r_{\rm in}, r_{\rm out})$ and $r = m_2(c, r_{\rm in}, r_{\rm out})$ for a fixed center c and size $\{r_{\rm in}, r_{\rm out}\}$. In the following we drop the subscript to alleviate the notation, since we are not yet interested in the type of measurement employed.

C. Statistical methods for the absence of HPs and the reliability of the simulations

In this subsection we present different hypothesis (labeled in Roman numerals) and statistical methodologies (labeled in arabic numbers) to search for HPs in the CMB. Once we have calculated $m(c, r_{\rm in}, r_{\rm out})$ for all the real and simulated CMB sky maps, we would like to see what are the similarities or dissimilarities between them. Therefore, given a sky map, we define $\mathscr{M}(r_{\rm in}, r_{\rm out})$ to be the set of all the measurements for a fixed size $\{r_{\rm in}, r_{\rm out}\}$ as,

$$\mathscr{M}^{\text{sky map}}_{r_{\rm in}, r_{\rm out}} = \{m(c, r_{\rm in}, r_{\rm out}) \mid c \in \mathbb{R}^2\ \} \qquad (5)$$

We want to test the similarity of the measurements from the real ($\mathscr{M}^{real}_{r_{\rm in}, r_{\rm out}}$) and the simulated sky maps ($\mathscr{M}^{sim}_{r_{\rm in}, r_{\rm out}}$) in two different regimes:

[2] They are defined according to an evenly-spaced grid.
[3] Instead of using the built in function *healpy.rotator.angdist()* to compute the angular distance $d(\mathcal{P})$, we implement our own function with *Numba* package, which is twice as fast.

I *Testing the reliability of simulated CMB sky maps for* $r_{out} \geq 0.035 : \mathscr{M}^{real}_{r_{in},r_{out}} \sim \mathscr{M}^{sim}_{r_{in},r_{out}}$ *on average.*

For this regime and according to CCC, the ring-like structures associated with HPs should not occur in the real CMB sky maps, so a similarity is expected between $\mathscr{M}^{real}_{r_{\rm in},r_{\rm out}}$ and $\mathscr{M}^{sim}_{r_{\rm in},r_{\rm out}}$, on average, with a p-value $p \geq 0.01$.

II *Testing the absence of HPs for* $r_{out} \leq 0.035$ $\mathscr{M}^{real}_{r_{in},r_{out}} \geq \mathscr{M}^{sim}_{r_{in},r_{out}}$ *on average.*

For this regime and according to CCC, HPs should be observable through their associated ring-like structures in the real CMB sky maps. Setting the non-existence of HPs as our null-hypothesis, we expect to find no proof of a larger amount of extreme negative slope measurements in $\mathscr{M}^{real}_{r_{\rm in},r_{\rm out}}$, or that $\mathscr{M}^{real}_{r_{\rm in},r_{\rm out}} \geq \mathscr{M}^{sim}_{r_{\rm in},r_{\rm out}}$ on average with a p-value $p \geq 0.01$. Failing to reject this hypothesis, the implication would be that manifestations of HPs are not observed in the CMB or that they are expected by ΛCDM. On the contrary, rejecting this hypothesis ($p < 0.01$) could give an indication towards the existence of HPs.

We calculate the statistics for both tests with four different methods:

1. *Kolmogorov-Smirnov (KS test):* this test is used to decide if a sample comes from a population with a specific distribution and is well-known in the literature. Some advantages of KS test are that it does not depend on the on the underlying cumulative distribution function being tested and it is a exact test. However, the main disadvantage is that it tends to be more sensitive at the bulk of the distribution than at the tails. Thus, we will compare these results with some other traditional and novel tests [1].

2. *Anderson-Darling (AD test):* it is a modified version of KS test, and it gives more weight to the tails. One of the main differences between both is that KS test is distribution free, while AD test does depend on the specific distribution. Another major difference is that AD test returns a list of critical values, rather than a single p-value like KS test, and this can provide the basis for a more thorough interpretation of the result. As an example, the null hypothesis of two samples coming from the same distribution is not rejected if $A^2 <$ than the critical value [4]. Hence, the main advantage of AD with respect to KS is a higher sensitivity and the main disadvantage is that the critical values need to be calculated every time, which is computationally expensive [1].

3. *Wilcoxon signed-rank (W test):* because the *Scipy* implementation of AD is only two-sided, we also employ W test which can be used as one-sided and two-sided test. W test is a non-parametric statistical test that compares two paired groups and it is well-known in the literature. Thus, it can be used to test the null hypothesis that two distributions have the same continuous distribution, returning a p-value [1].

When we perform a certain test t for a fixed annulus size $\{r_{\rm in}, r_{\rm out}\}$, we compute the similarity between a single real map $\mathscr{M}^{real}_{r_{\rm in},r_{\rm out}}$ against $N = 1000$ simulated maps $\mathscr{M}^{sim}_{r_{\rm in},r_{\rm out}}$ and we obtain a set of p-values or in the case of AD test, a set of critical values. We define the set of p-values (or AD critical values) as,

$$P_{\rm t,i}(r_{\rm in}, r_{\rm out}) = \{p(x,i) \mid x \in \mathscr{M}^{sim}_{r_{\rm in},r_{\rm out}}\} \text{ for } i \in \{1,4\}, \quad (6)$$

where i refers to the four real sky maps presented in Section III, and t to the type of test performed. From the a single set $P_{\rm t,i}(r_{\rm in}, r_{\rm out})$ we calculate the mean and the standard error $\mu(P_{\rm t,i}(r_{\rm in}, r_{\rm out})) \pm \varepsilon(P_{\rm t,i}(r_{\rm in}, r_{\rm out}))$ at confidence interval (CI) of 95%. If for a given size $\{r_{\rm in}, r_{\rm out}\}$ we were to find $\mu(P_{\rm t,i}(r_{\rm in}, r_{\rm out})) \lesssim 0.01$ for $t =$KS test, W test and/or $\mu(P_{\rm t,i}(r_{\rm in}, r_{\rm out})) \lesssim$ AD critical value at 1% significance level for AD test, this could give an indication towards the existence of HPs. Nonetheless, these traditional methods are not commonly used on the search of HPs in the real CMB sky map. Instead, another methodology is implemented by [7, 15] :

4. *A-functions:* this method was proposed in [17] to overcome the sensitivity problems of KS test. These functions are defined as follows,

$$A^{+}(r_{\rm in}, r_{\rm out}) = -\frac{j}{N}\sum_{i=1}^{N} log(1 - F_{\hat{a}}(r_{\rm in}, r_{\rm out})^{j}), \quad (7)$$

$$A^{-}(r_{\rm in}, r_{\rm out}) = -\frac{j}{N}\sum_{i=1}^{N} log(1 - [1 - F_{\hat{a}}(r_{\rm in}, r_{\rm out})]^{j}), \quad (8)$$

where $F_{\hat{a}}(r_{\rm in}, r_{\rm out})$ is the cumulative distribution function (CDF) of the normalized slope $\hat{a}$ for all centers c and j is a positive real number that represents the relative weight of tails of the distribution. Distributions with an excess of extreme positive or negative values will reflect this with a large $A^{+}(r_{\rm in}, r_{\rm out})$ or $A^{-}(r_{\rm in}, r_{\rm out})$, respectively.

Because we want to compare the performance of the A functions with the traditional tests, we follow the previous works [7, 15]. The methodology

[4] *Scipy* library returns directly the statistic A^2. This implementation is only two-sided but the test itself can also be one-sided.

is as follows: the authors computed the A functions setting $j = 10,000$ for each $\mathscr{M}^{sim}_{r_{\rm in},r_{\rm out}}$ and $\mathscr{M}^{real}_{r_{\rm in},r_{\rm out}}$, returning $\{A^+_{\rm sim}(r_{\rm in},r_{\rm out}), A^-_{\rm sim}(r_{\rm in},r_{\rm out})\}$ and $\{A^+_{\rm real}(r_{\rm in},r_{\rm out}), A^-_{\rm real}(r_{\rm in},r_{\rm out})\}$.

- If $A^-_{\rm sim}(r_{\rm in},r_{\rm out}) > A^-_{\rm real}(r_{\rm in},r_{\rm out})$ the counter $N^-(r_{\rm in},r_{\rm out})$ increases one unit
- If $A^+_{\rm sim}(r_{\rm in},r_{\rm out}) > A^+_{\rm real}(r_{\rm in},r_{\rm out})$ the counter $N^+(r_{\rm in},r_{\rm out})$ also increases one unit.

Distributions with an excess of extreme values reflect this with large $A^+(r_{\rm in},r_{\rm out})$ and $A^-(r_{\rm in},r_{\rm out})$. Therefore, if for a certain size we find a counter $N^+(r_{\rm in},r_{\rm out}) \sim 0$, this would mean a large excess of positive measurements, which is not expected by CCC. If $N^-(r_{\rm in}, r_{out} \leq 0.035) \sim 0$, it reflects that $\mathscr{M}^{real}_{r_{\rm in},r_{\rm out}}$ has the largest population of negative extreme measurements, implying the existence of HPs.

D. Statistical methods for the location of HPs

Note that the A functions and the previous methods test the presence or absence of HPs, but not their locations. Moreover, we assume that the population of HPs is large enough to generate an excess of very extreme negative measurements, but we do not take into account the possibility that HPs are rare in the CMB. To be able to locate HPs in this case we propose yet another test, whose aim is to store the location information of each anomaly.

III *Location of HP candidates (HPC) at α significance level*

Because we have simulated $N = 1000$ CMB sky maps, for a given center c and a size $\{r_{\rm in},r_{\rm out}\}$ we have a set of N measurements $m(c,r_{\rm in},r_{\rm out})$ defined as:

$$\mathbb{M}(c,r_{\rm in},r_{\rm out}) = \{m_i(c,r_{\rm in},r_{\rm out}) \mid i \in \text{ simulated sky maps}\} \quad (9)$$

When sorting this set by increasing value and defining a certain α significance level, we obtain the set of the most extreme negative values $e^{sim}(c,r_{\rm in},r_{\rm out}) \subset \mathbb{M}(c,r_{\rm in},r_{\rm out})$ as follows:

$$e^{sim}(c,r_{\rm in},r_{\rm out}) = sort(\ \mathbb{M}\ (c,r_{\rm in},r_{\rm out}))[\leqslant \alpha/2] \quad (10)$$

Regarding the real CMB sky maps, for this particular location c and size $\{r_{\rm in},r_{\rm out}\}$ we have four measurements $m_i(c,r_{\rm in},r_{\rm out})$, where i refers again to the real CMB sky maps. If for a certain real sky map i the measurement $m_i(c,r_{\rm in},r_{\rm out})$ lays inside set $e^{sim}(c,r_{\rm in},r_{\rm out})$, then we consider this annulus $\mathcal{A}(c,r_{\rm in},r_{\rm out})$ a HPC. Otherwise, it will not be considerate a candidate (NHPC). Note that the annulus is a function of $\{r_{\rm in},r_{\rm out}\}$, so we are able to locate it in the sky map. Finally we compute the rate of HPC, defined as the number of HPC over the total number of locations c explored in percentage. We expect to find a HPC rate of $\alpha/2$ due to statistical fluctuations, but larger rate deviations would imply the existence of HPs.

A similar procedure can be employed to measure the population in the upper tail, just by ordering $\mathbb{M}(c,r_{\rm in},r_{\rm out})$ by decreasing value. It is important to note that this procedure does not only point at HPC if they are anomalies in our data, but also locates them in the real CMB sky map.

E. Statistical methods for the reliability of the methodology

As a further proof of the performance of our methodology, we want to test whether we are able to capture ring-like structures with an artificial data set by employing the same methodology as Section IV D.

To address this issue we generate 1000 simulated CMB sky maps, and 110 artificial annuli (AA), sampled from the same Gaussian distribution, are injected. Because we are unaware of how visible HPs are, we create 6 different types of AA to assess the performance of our method for more and less visible AA. In Fig. 2 we plot in solid line the portions of the Gaussians employed to create six different types of AA. This curve is revolved around to create a surface of revolution, which is projected in the simulated sky map as a 2D AA. Note that the locations of AA are completely random. Moreover, due to the fact that potential HPs sizes are unknown, the size of the AA is also random, with a limit $r_{\rm out} \leq 0.07$ rad.

A single simulation is cloned 6 times to insert a single type of AA per sky map. We store their locations and scan the maps, obtaining a population of measurements m. After that, we build a confidence interval of the population at a certain α significance level to select the most negative measurements, as we explained in Section IV D. Because each extremely negative measurement has a certain location c and size $\{r_{\rm in},r_{\rm out}\}$, we can count how many of these corresponding annuli intersect a single AA. If a single extremely negative annulus intersects an AA, then the AA is detected and labeled as such. Otherwise, we classify it as a *fake AA*.

We want to measure the performance of our method in terms of the confusion matrix (see Table I). It is important to note that the amount of false positive (FP) is determined by the significance level α.

Due to the fact that we are not interested in the correct classification of fake AA, i.e. TN are neglected, we will measure the performance in terms of the True Positive Rate (TPR), False Negative Rate (FNR), Positive Predictive Value (PPV) and False Discovery Rate (FDR).

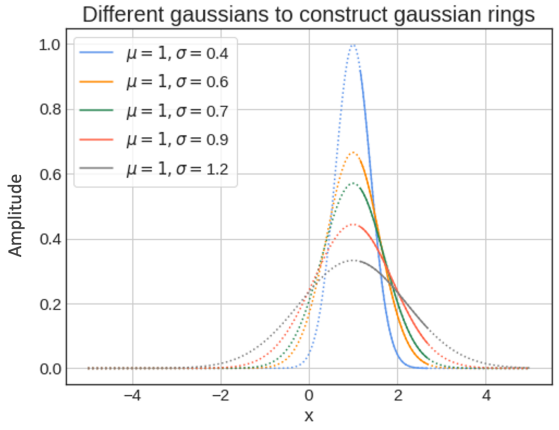

FIG. 2: We plot the Gaussian distributions employed to construct AA. The solid line represents the portion of the Gaussian that has been rotated in the vertical axis to form a surface of revolution. Afterwards, this 3D surface was projected in a 2D simulated sky map.

TABLE I: Confusion matrix for artificial annuli (AA) and fake artificial annuli (fake AA)

		Actual class	
		AA	*Fake AA*
Predicted class	*AA*	True positive (TP)	False positive (FP)
	Fake AA	False negative (FN)	True negative (TN)

$$TPR = \frac{TP}{TP + FN} \tag{11}$$

$$FNR = \frac{FN}{FN + TP} = 1 - TPR \tag{12}$$

$$PPV = \frac{TP}{TP + FP} \tag{13}$$

$$FDR = \frac{FP}{FP + TP} = 1 - PPV \tag{14}$$

To enlighten the computations, for each CMB sky map we only compute TPR and PPV, because FNR and FDR can be derived from them, respectively.

V. RESULTS

In this section we present the results of testing the reliability of the simulations, and the absence of HPs in the CMB sky map sky map. We employ Commander-Ruler map (sky map 1) and 1000 simulated CMB maps. Different cleaned maps, such as SMICA, NILC and SEVEM, yield equivalent results.

A. On the reliability of the similated CMB maps

To test the quality of the simulations we compare N $\mathscr{M}^{\rm sim}_{r_{\rm in},r_{\rm out}}$ against $\mathscr{M}^{\rm real}_{r_{\rm in},r_{\rm out}}$ of Commander-Ruler, in the region where $r_{\rm out} \geq 0.035$, i.e. where HP are not present according to CCC. Thus, we compute KS test with the hypothesis that $\mathscr{M}^{\rm sim}_{r_{\rm in},r_{\rm out}}$ distributions are equal to $\mathscr{M}^{\rm real}_{r_{\rm in},r_{\rm out}}$, with a significance level $\alpha = 0.01$.

After performing the test we obtain a distribution of 1000 p-values, namely $P_{KS,1}$. We compute the mean of the distribution, $\mu(P_{KS,1})$, and its error at 95% CI, $\varepsilon(P_{KS,1})$. Assuming that the simulations of CMB are very similar to the real sky maps it would be expected that for this test we would obtain a large $\mu(P_{KS,1})$, meaning that we have a good agreement with real CMB sky maps. Nonetheless, we find instead that the mean of the set of p-values $\mu(P_{KS,1}) < 0.1$ at 95% CI. Moreover, when considering also the standard error $\mu(P_{KS,1}) \pm \varepsilon(P_{KS,1})$, its value is at most ≈ 0.15. Furthermore, when increasing the width of the annuli $(r_{\rm out} - r_{\rm in})$, the value of $\mu(P_{KS,1})$ is reduced even further, and it is expected to continue decreasing as we increase the width of the annuli.

As we mentioned before, AD and W tests yield equivalent results and this behaviour is common for all real sky maps. One may think that this may be due to the low number of pixels in the annuli. However, in this region we explored large annuli of $\sim 14,000$ pixels.

B. On the generation and detection of artificial HPs

Due to the disagreement between data and simulations in the region where $r_{\rm out} \geq 0.035$, we generate a simple data set to measure the reliability of the methodology developed in this work. As we have explained in Section IV E, we simulate 1000 artificial maps. Because we have 6 Gaussian distributions, which yields 6 different types of slopes, the computations for a single simulated CMB sky map are performed 6 times, (one for each Gaussian distribution).

Once we have generated the maps, we scanned them with our procedure and we computed for each map the normalized slope and Pearson correlation coefficient (see IV E). In Fig. 3 and Fig. 4 we plot the mean TPR and the mean PPV as functions of the significance level α for three different slopes of AA, i.e. sampled from three different Gaussian distributions (see Fig. 2).

From Fig. 3 can observe that as we increase σ, the TPR and the PPV decrease. We speculate that for large σ, the TPR of $m_2(c, r_{\rm in}, r_{\rm out})$ would be slightly better than $m_1(c, r_{\rm in}, r_{\rm out})$, because $m_2(c, r_{\rm in}, r_{\rm out})$ points out at the strongest correlations on the data. Note that, FNR has a complementary behaviour to TPR. In Fig. 4, we conclude that $m_2(c, r_{\rm in}, r_{\rm out})$ is less precise $m_1(c, r_{\rm in}, r_{\rm out})$, with a $\sim 20\%$ difference for all α. Nevertheless, with both measurements we are able to detect most of the rings (around 95% TPR).

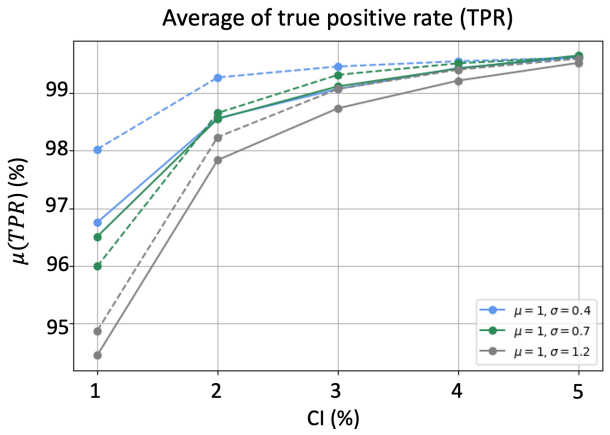

FIG. 3: Average TPR as a function of the significance level α for different Gaussian rings. The solid line represents the results of Pearson coefficient $m_2(c, r_{\rm in}, r_{\rm out})$ and the dotted line shows the results of the normalized slope $m_1(c, r_{\rm in}, r_{\rm out})$.

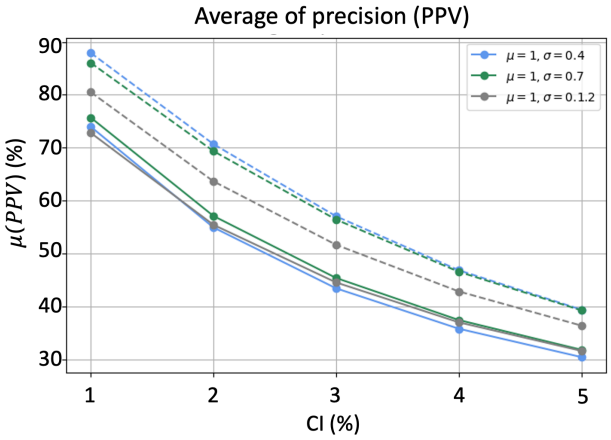

FIG. 4: Average PPV as a function of the significance level α for different Gaussian rings.The solid line represents the results of Pearson coefficient $m_2(c, r_{\rm in}, r_{\rm out})$ and the dotted line shows the results of the normalized slope $m_1(c, r_{\rm in}, r_{\rm out})$.

C. On the absence of HPs in the CMB

To test the absence of HPs in the CMB, we compare again $N = 1000$ samples $\mathscr{M}^{\rm sim}_{r_{\rm in},r_{\rm out}}$ against $\mathscr{M}^{\rm real}_{r_{\rm in},r_{\rm out}}$ of Commander-Ruler with KS test at $\alpha = 0.01$ significance level. Moreover, we test whether the simulations contain more negative values than the real sky map by testing the hypothesis $\mathscr{M}^{\rm real}_{r_{\rm in},r_{\rm out}} \geq \mathscr{M}^{\rm sim}_{r_{\rm in},r_{\rm out}}$. We do not find any $\mu(P_{KS,1}) < 0.01$, but one of the lowest mean p-values is $\mu(P_{KS,1}(r_{\rm in} = 0.02, r_{\rm out} = 0.03)) = 0.19$, which points at the same annulus size as Penrose et al. indicate in [7]. A possible explanation for low mean p-values might be that there are not as many HPs that produce a significant excess of negative measurements as expected by CCC.

For completeness, we calculate the counters $N^{-}_{r_{\rm in},r_{\rm out}}$ and $N^{+}_{r_{\rm in},r_{\rm out}}$ for the normalized slope $\hat{a}$, with the A functions setting $j = 10000$. As we discussed before, this methodology was proposed to give more importance to the tails of the distribution, due to the fact that KS test gives more weight to the bull instead (see Section IV C). When computing $N^{-}_{r_{\rm in},r_{\rm out}}$ and $N^{+}_{r_{\rm in},r_{\rm out}}$ we did not find enough statistical significance for $\alpha = 1\%$ and we were unable to reproduce the results from [7], where they claimed to have identified HPs at a 99.98% confidence level. Contrary to A functions, AD test, W test and KS test results' are in agreement. The importance of this lies in the fact that AD test, which is a generalization of KS test, gives more importance to the tails of the distribution than to the bulk, like A functions. Therefore, we conclude that for the particular task at hand, AD test is a more robust methodology to assess the presence or absence of HPs in the CMB sky maps.

In spite of this, none of the traditional tests employed proved the existence of HPs in the real CMB.

D. On the location of HPs in the CMB

Next, we intend to build a confidence interval to obtain the most negative measurements, as we have shown in Section IV D, under the assumption that the simulations represent the real CMB sky maps. In [7] and [19] it is stated that HPs should have extremely negative measurements [5], but we do not have a theoretical threshold for this value. Therefore, assuming the simulations are representative of the real CMB sky maps, we compute different confidence intervals for $\alpha = [1\%, 5\%]$.

When we employ the measurement $m_1(c, r_{\rm in}, r_{\rm out})$, we were unable to find deviations of the HPC rate $> \alpha/2$. Furthermore, as we increase the size of the annuli, we observe that the HPC rate decreases specially for $r_{\rm out} \geq 0.035$. The main implication of this is that as we increase the size of the rings above the theoretical threshold $r_{\rm out} \geq 0.035$, the possibilities of detecting an *extremely negative value* (a HPC) decrease. Another important issue is the fact that as we increase the size of the annuli, the simulated CMB sky maps deviate further form the real ones, as we discussed in V A.

When we employ the measurement $m_2(c, r_{\rm in}, r_{\rm out})$, for $\alpha = 5\%$ it is expected to have at most a deviation of 2.5%, but we obtained deviations of 3.2%, 2.9% and 2.8% for $(r_{\rm in} = 0.010, r_{\rm out} = 0.015)$, $(r_{\rm in} = 0.005, r_{\rm out} = 0.015)$ and $(r_{\rm in} = 0.000, r_{\rm out} = 0.015)$, respectively. An interesting fact is that these deviations coincide among all the real CMB sky maps. Moreover, these deviations are higher than the ones found for $m_1(c, r_{\rm in}, r_{\rm out})$ at 5%

[5] We also explored the extremely positive measurements for completeness but no interesting results were found.

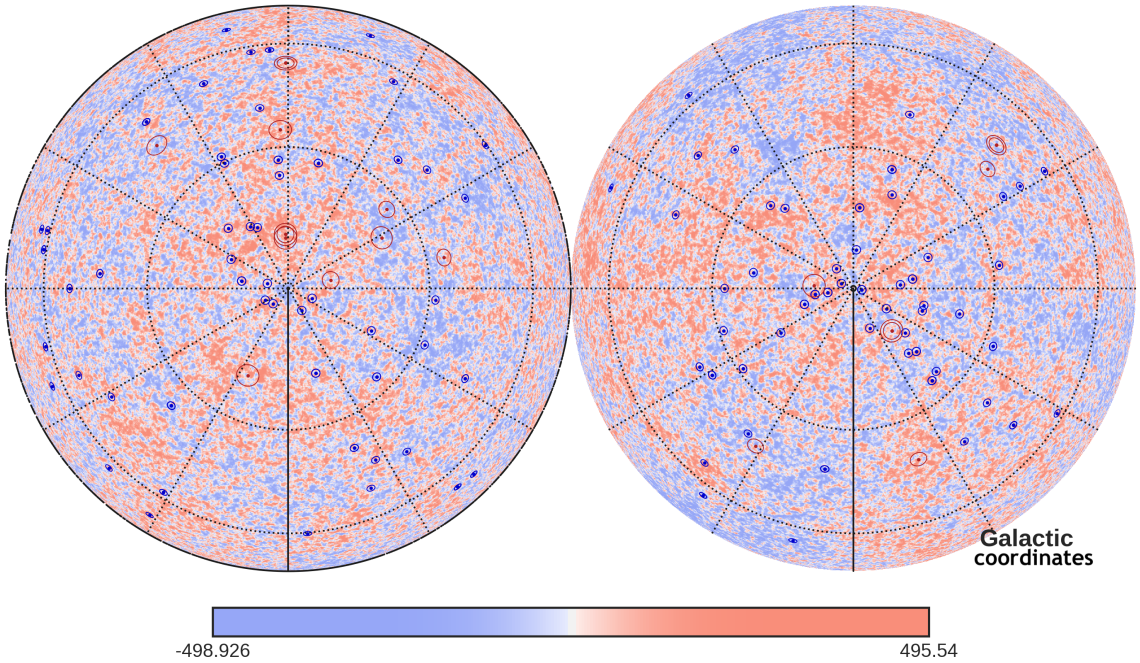

FIG. 5: *HPC obtained with Pearson coefficient r measurement at 5% significance level, represented in orthographic projection:* in dark red we plotted the most negative annuli presented in [7], while in dark blue we plot HPC found by our confidence interval. The background CMB sky map corresponds to Commander-Ruler sky map.

confidence interval, which were at most $\sim 2.6\%$.

In Fig. 5 we plot in dark red the most negative annuli indicated by the authors in [7], and in blue we plot the HPC found by our methodology for 5% significance level. As we can observe, red and blue annuli do not coincide, because the methodology presented in [7] employs the CMB sky map at 70GHz, rather than the pre-processed maps.

VI. CONCLUSION

The main goal of this work was to search for ring-like anomalies in the CMB. Because we are searching for linear relationships between the measured temperature T and the angular distance d in an annulus, we measure the normalized slopes $\hat{a} = m_1(c, r_{\rm in}, r_{\rm out})$ and Pearson coefficients $r = m_2(c, r_{\rm in}, r_{\rm out})$ of 12800 locations for different $\{r_{\rm in}, r_{\rm out}\}$ sizes (see Fig. 1). The measurements are performed on real and simulated CMB sky maps. We compare both distributions of measurements to draw conclusions about the reliability of the simulations and the absence of HPs in the CMB.

In this study, when measuring the quality of the simulations employed, we observed a mismatch between the real CMB maps and the simulations, in the region where ring-like structures associated with HPs are not expected. A potential cause for this difference would be that the underlying temperature field distribution of the CMB is not being considered when performing the simulations.

The results show that the simulations departed from real CMB sky maps. Due to this fact, we were unable to quantify the performance of our methodology to detect ring-like structures. To overcome this obstacle, we constructed an artificial data set to assess the performance of our algorithm, and we detected artificial annuli with a $TPR \sim 95\%$. However, future work should address the reason for the difference between simulation and real CMB sky maps.

In this study we also postulated the absence of the ring-like manifestations of HPs in the CMB, and we were unable to statistically reject this hypothesis. However, we theorize that because the amount of HPs in the CMB is very low, it may not be possible to say anything about their existence with the currently available simulation algorithms.

To treat HPs as anomalies in the CMB, from simulated sky maps we generated CI for $m(c, r_{\rm in}, r_{\rm out})$ at different significance levels α. When setting the confidence interval at $s\%$ significance level we were expecting (in absence of HPs) deviations of at most $s/2$ due to the randomness of the data, so we search for deviations larger than this value. We found deviations $> 2.5\%$ for $m_2(c, r_{\rm in}, r_{\rm out})$ at 95% significance level, which implies that there are more negative measurements in the real CMB sky maps than in the simulations. Nevertheless, as mentioned before, this study is not conclusive due to the mismatch between the simulated and real CMB sky maps, as the CI relies on the simulations performed.

We also employed KS, W and AD tests to investigate the existence of HPs and the reliability the *A-functions* (see Section IV C). KS, W and AD tests gave equiva-

lent results, while *A-functions* gave results which are not statistically significant. An interesting alternative to the *A-functions* is AD tests, since it is a generalization of the well known KS test and it does give more weight to the tails of the distribution. Moreover, it is important to note that *A-functions* need to be tuned manually, so different parameters might yield different results for the same test.

Finally, we foresee a possibility to apply the methodology presented in this article to search for imprints of HPs in the Cosmological Gravitational wave Background (CGB). In such an approach, a key difference between CMB and CGB sky maps needs to be taken into account: whereas the CMB was created at the fixed moment of Recombination and thus allows for a straightforward prediction of the maximum size the rings, no such crisp moment of time can be identified for the CGB. However, the current generation of gravitational wave (GW) detectors are designed to detect gravitational waves emanating from binary black holes created predominantly at red-shifts $z \sim [3, 6]$. We expect that this is sufficiently precise to allow for a prediction of the size of rings found in the CGB. Once the amount of binary black holes detections has increased enough to make for an accurate CGB sky map, we expect the methodology presented in this paper to be applicable to search for evidence of HPs in the CGB. It will be interesting to see whether the rings found in the CGB share the same centres as the candidates found in the CMB. If so, it would constitute additional evidence that the rings found in the CMB are not statistical artifacts, and would serve as an independent indication for the existence of HPs.

VII. ACKNOWLEDGEMENT

We would like to express our great appreciation to Sir Roger Penrose for proposing this line of research. We gratefully thank Q. Meijer for for the fruitful and inspiring discussions during this study, and S. Caudill for the critical reading of the manuscript and her constructive inputs. M.L. is supported by the research program of the Netherlands Organisation for Scientific Research (NWO).

[1] Probability and Statistics for Engineers and Scientists. Pearson Education, 2007.

[2] Planck public data release 2 maps, `https://irsa.ipac.caltech.edu/data/Planck/release_2/all-sky-maps/matrix_cmb.html`, (accessed 26th May 2020).

[3] D. Contreras A. DeAbreu and D. Scott. Searching for concentric low variance circles in the cosmic microwave background. JCAP, 12:031, 2015.

[4] A. Challinor A. Lewis and A. Lasenby. Efficient computation of CMB anisotropies in closed FRW models. Astrophys. J. , 538:473–476, 2000.

[5] A. Hall C. Howlett, A. Lewis and A. Challinor. CMB power spectrum parameter degeneracies in the era of precision cosmology. JCAP, 1204:027, 2012.

[6] K. A. Meissner D. An and P. Nurowski. Structures in the Planck map of the CMB. 7 2013.

[7] P. Nurowski D. An, K. Meissner and R. Penroser. Apparent evidence for Hawking points in the CMB Sky. Mon. Not. Roy. Astron. Soc., 495(3):3403–3408, 2020.

[8] A. Zonca et al. healpy: equal area pixelization and spherical harmonics transforms for data on the sphere in python. Journal of Open Source Software, 4(35):1298, March 2019.

[9] K. M. Górski et al. HEALPix: A Framework for High-Resolution Discretization and Fast Analysis of Data Distributed on the Sphere. Astrophys. J. , 622:759–771, April 2005.

[10] P. A. R. Ade et al. Planck 2013 results. xxiii. isotropy and statistics of the cmb. Astronomy and Astrophysics, 594:1–62, 2014.

[11] Planck Collaboration N. Aghanim et al. Planck 2018 results. vi. cosmological parameters. arXiv: Cosmology and Nongalactic Astrophysics, 2018.

[12] Krzysztof M Gorski, Benjamin D Wandelt, Frode K Hansen, Eric Hivon, and Anthony J Banday. The healpix primer. arXiv preprint astro-ph/9905275, 1999.

[13] V. G. Gurzadyan and R. Penrose. Concentric circles in WMAP data may provide evidence of violent pre-Big-Bang activity. 11 2010.

[14] V. G. Gurzadyan and R. Penrose. On CCC-predicted concentric low-variance circles in the CMB sky. Eur. Phys. J. Plus, 128:22, 2013.

[15] D. L. Jow and D. Scott. Re-evaluating evidence for Hawking points in the CMB. JCAP, 03:021, 2020.

[16] P. Nurowski K. A. Meissner and B. Ruszczycki. Structures in the microwave background radiation. Proceedings of the Royal Society A: Mathematical, Physical and Engineering Sciences, 469, 2013.

[17] K. A. Meissner. A tail sensitive test for cumulative distribution functions. 2012.

[18] R. Penrose. The road to reality : a complete guide to the laws of the universe. Vintage, London, 2005.

[19] R.Penrose. Cycles of Time: An Extraordinary New View of the Universe. Knopf Doubleday Publishing Group, 2011.

[20] A. Pitrou S. Lam and S. Seibert. Numba: a llvm-based python jit compiler. pages 1–6, 11 2015.

[21] I. K. Wehus and H. K. Eriksen. A SEARCH FOR CONCENTRIC CIRCLES IN THE 7 YEAR WILKINSON MICROWAVE ANISOTROPY PROBE TEMPERATURESKY MAPS. The Astrophysical Journal, 733(2):L29, may 2011.